Journal of Materials Chemistry A

Accepted Manuscript

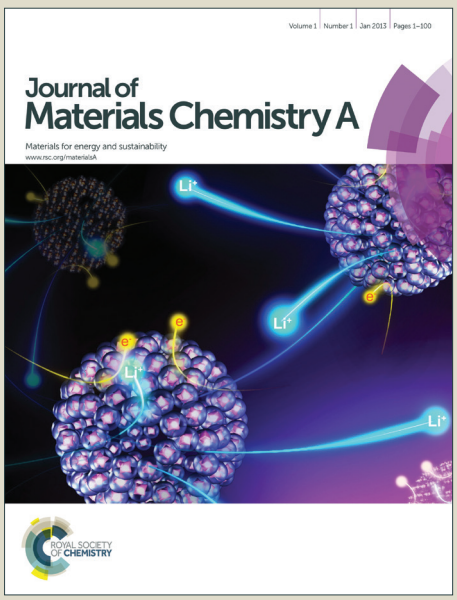

ROYAL SOCIETY OF CHEMISTRY

www.rsc.org/materialsA

Cite this: DOI: 10.1039/c0xx00000x

www.rsc.org/xxxxxx

ARTICLE TYPE

Plasmon enhanced efficient dye-sensitized solar cells using core-shell-structured β-$NaYF_4$:Yb,Er@SiO_2@Au nanocomposites†

Peng Zhao, Yihua Zhu,* Xiaoling Yang, Xin Jiang, Jianhua Shen and Chunzhong Li*

Received (in XXX, XXX) Xth XXXXXXXXX 20XX, Accepted Xth XXXXXXXXX 20XX

DOI: 10.1039/b000000x

Core-shell-structured β-$NaYF_4$:Yb,Er@SiO_2@Au nanocomposites have been successfully prepared and applied for the first time as a multifunctional layer on top of the transparent TiO_2 layer in dye-sensitized solar cells (DSSCs). Structural characterizations indicate that $NaYF_4$:Yb,Er@SiO_2 nanoparticles (NPs) have an averge size of 300 nm in length and 230 nm in width. By adding these large dimension NPs as effective light scattering centers and upconversion centers, the performance of DSSCs was enhanced and the energy conversion efficiency of 7.56% was achieved. Furthermore, attachment of ~20 nm Au NPs on the surface of $NaYF_4$:Yb,Er@SiO_2 NPs could further improve the performance of DSSCs, resulting in efficiency of 8.23%, which is a noticeable enhancement of 14.78% compared to the cell without the multifunctional layer. Therefore, this work provides an insight to possible further optimize the efficiency of DSSCs.

1. Introduction

Dye-sensitized solar cells (DSSCs) have drawn intense attention of both academic and industrial fields for decades owing to their high-efficiency and potential for manufacture at a low-cost.[1,2] Over the past decades, extensive efforts have been focused on the improvement of its photoelectric conversion efficiency by optimizing the structure and properties of the photoanode.[3-5] Generally, the conventional photoanode of DSSCs is composed of TiO_2 nanoparticles (NPs) with a size of 20-40 nm. However, due to their small size, the scattering effects are negligible for visible light, and hence a large proportion of incident light would not be utilized, resulting in a low light harvesting efficiency.[6] To date, one effective way to enhance the light harvesting capability is to introduce the scattering layer on top of the transparent TiO_2 layer.[7-9]

Currently, Ru complexes, such as N3 and N719, are known as the best sensitizers in DSSCs. However, the main absorption wavelength ranges for dyes N3 and N719 are only up to < 700 nm, which are very low compared to the near-infrared (NIR) light.[10] About 43% of the radiant energy from the sun in the infrared region is not absorbed, which limits the sun energy conversion efficiency of DSSCs. An alternative way to improve light harvesting and thereby the efficiency of the solar cells can be the utilization of upconversion phosphors (UCPs).[11,12] The UCPs, which can convert low-energy photons (near infrared photons) into high-energy photons (visible to ultraviolet photons) via the multiphoton processes, have been considered as one of the promising solutions and have been applied in DSSCs.[13-17] Among all the upconversion materials, due to low phonon energy of lattices, hexagonal phase sodium yttrium fluoride (β-$NaYF_4$) crystals have been reported to be one of the most efficient upconversion host materials and have been widely studied, especially for the systems doped with Yb/Er and Yb/Tm.[18-22] It is known that smaller $NaYF_4$ UCPs with increased surface defects and ligands with high-energy vibrational modes can lead to a serious quenching effect.[23-25] Therefore, when small $NaYF_4$ UCPs were used in TiO_2 film internally, defects and ligands on the surface of them will act as trapping centers and large part of photoinduced electrons can be trapped, leading to a heavy loss of photocurrent and which become the major limitation for their application in DSSCs internally.[17] To overcome this drawback indirectly, Zhao et al. proposed a novel core/double-shell β-$NaYF_4$@SiO_2@TiO_2 structure for NIR light harvesting and light reflecting,[26] resulting an efficiency of 8.65%. This work paved a facile way to enable large dimension β-$NaYF_4$ UCPs to be used as scattering and upconversion centers in photoanodes.

More recently, localized surface plasmon resonance (LSPR) from metallic nanostructure has been introduced into DSSCs to enhance light absorption and photocurrent generation.[27-31] The noble metal NPs act as light harvesting components *via* excitation of their LSPR in the visible range of spectrum. Meanwhile, the coupling of LSPR with the adsorbed dye will lead to an increase in the effective absorption cross-section of dye molecules.[32] Noble metal NPs have been observed to improve light harvesting in thin film solar cells where metal NPs are dispersed as islands.[33] Ogale et al. had *in situ* loaded Au NPs on TiO_2 nanofibers as the light harvesting layer, a remarkable enhancement in the efficiency was achieved. The authors had demonstrated that coupled surface plasmon-polariton modes played a key role to the enhancement.[34] Additionally, the incorporation noble metal NPs with UCPs could significantly enhance the upconversion fluorescence emission, which could make a better use of UCPs as upconversion centers in DSSCs.[35,36]

Herein, in this report, we present a facile method to integrate

β-$NaYF_4$:Yb,Er UCNPs with Au NPs for constructing core-shell-structured $NaYF_4$:Yb,Er@SiO_2@Au hybrid nanocomposites. A uniform modified silica layer on $NaYF_4$:Yb,Er NPs serves as an interface for Au decoration and an isolating layer to prevent bare UCNPs act as serious recombination centers causing loss of the photocurrent. Figure 1 illustrates the experimental process for preparation of $NaYF_4$:Yb,Er@SiO_2@Au hybrid nanocomposites and the configuration of DSSCs. For device application, the obtained nanocomposites were applied for proof-of-concept study in DSSCs as a multifunctional layer on top of the transparent TiO_2 layer. By utilization of these efficient $NaYF_4$:Yb,Er UCNPs, NIR irradiation can be absorbed and harvested indirectly by dye molecules to broaden the absorption region and produce more electrons, and these large nanocomposites could also be used as effective scattering centers, which scatter light by multiple reflections, increasing their optical path-length.[10] Furthermore, the LSPR effects from Au NPs could not only enhance the upconversion emission but also excite dye molecules more effectively than incident far-field light, thus leading to enhanced light adsorption and photocurrent generation in DSSCs.[37]

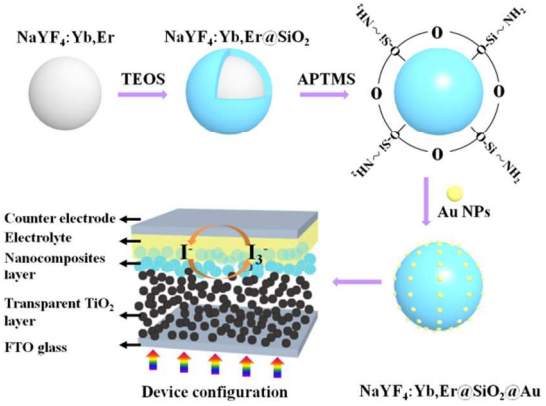

Figure 1. Schematic for the experimental process for core-shell-structured β-$NaYF_4$:Yb,Er@SiO_2@Au nanocomposites and the configuration of DSSCs device.

2. Experimental

2.1 Materials

$RE(NO)_3$ (99.9%) (RE = Y, Yb, Er), tetraethyl orthosilicate (TEOS), 3-Aminopropyltrimethoxysilane (APTMS) and Poly(acrylic acid) (PAA) were obtained from Alfa Aesar Co. Ltd., Chloroauric acid, Dye sensitizer cis-bis(isothicyanato)bis(2, 2'-bipyridyl-4, 4'-discarboxylato)-ruthenium (II)-bis-tetrabutylammonium (coded as N719), terpineol, ethyl cellulose, LiI, 4-tert-butylpyridine (TBP) and chloroplatinic acid were purchased from Sigma-Aldrich Chemicals Co., all other chemicals were purchased from the Shanghai Chemical Reagent Co.. All chemicals were used as received.

2.2 Synthesis of carboxyl-modified β-$NaYF_4$ UCNPs

Carboxyl-modified β-$NaYF_4$ UCNPs were prepared by adapting the method we reported before.[38,39] Typically, 1.2 mmol of $RE(NO_3)_3$ (Y:Yb:Er = 80:18:2), 2.4 mmol of NaCl and 1.8 g of PAA were dissolved in 20 mL ethylene glycol (EG) and mixed thoroughly to form a transparent solution. Then NH_4F (5 mmol) dissolved in 15 mL EG was added to the above mixture under stirring. The resulting mixture was transferred into a 50 mL Teflon-linked autoclave, which then sealed and heated to 200 ºC for 12 h. After cooling down to room temperature, the products were collected by centrifugation, washed with ethanol and ultrapure water several times, and dried in an oven at 60 ºC.

2.3 Synthesis of amimo-modified $NaYF_4$:Yb,Er@SiO_2 NPs

In a typical modified Stöber sol–gel process synthesis of $NaYF_4$:Yb,Er@SiO_2 particles. 50 mg of as-obtained $NaYF_4$:Yb,Er UCNPs were dispersed in a solution containing 80 mL of ethanol and 20 mL of ultrapure water, then sonicated at room temperature for 30 min. Then, a solution of 2 mL of 28% ammonia solution was added to the mixture, followed by dropwise addition of 20 μL of TEOS and the reaction proceeded for 8 h under continuous stirring. Then, 200 μL of APTMS was added and allowed to react for another 1 h, yielding amimo-modified core-shell structured $NaYF_4$:Yb,Er@SiO_2 NPs. Finally, the products were centrifuged with ethanol and ultrapure water several times and dried at 60 ºC for further use.

2.4 Synthesis of $NaYF_4$:Yb,Er@SiO_2@Au hybrid composites

Citrate-stabilized Au NPs of 20 nm were prepared according to the reported methods.[40] To prepare $NaYF_4$:Yb,Er@SiO_2@Au hybrid nanocomposites, 1 mL suspension of $NaYF_4$:Yb,Er@SiO_2 NPs (1 mM) was swiftly added into a 2 mL suspension of Au NPs (1 mM), after being vigorously rotated for 5 min, the mixed solution was sealed in a 10 mL plastic tube and slowly rotated for another 2 h.

2.5 Device fabrication

TiO_2 (20-40 nm) paste for transparent layer was prepared by hydrolysis of titanium tetraisopropoxide *via* the reported procedure.[41] In order to obtain the paste for scattering layer, previously obtained all samples were added into the solution containing terpineol (1 mL), ethyl cellulose (25 mg) and Triton X-100 (0.4 mL) and stirring for 1 h. Doctor blade method was used to prepare photoelectrodes followed by sintering at 450 ºC for 30 min. For dye adsorption, films were immersed in anhydrous ethanol solution of N719 dye (0.5 mM) for 24 h at room temperature. The liquid electrolyte was comprised of LiI (0.1 M), I_2 (0.05 M) and TBP (0.5 M) in acetonitrile. The platinum counter electrode was prepared by spin-coating H_2PtCl_6 (in isopropanol, 15 mM) onto the FTO glass followed by heating at 400 ºC for 30 min.

2.6 Characterization

To demonstrate the overall uniformity and morphology of the particles, the samples were characterized by scanning electron microscopy (SEM) using JEOL SM-6360LV microscope equipped with an energy dispersive X-ray spectroscopy (EDS). Transmission electron microscopy (TEM) images were taken with a JEOL 2011 microscope (Japan) operated at 200 kV. The crystal structure was investigated by X-ray power diffraction (RIGAK, D/MAX 2550 VB/PC, Japan). Fluorescence spectra were measured on a Fluorolog-3-P UV-VIS-NIR fluorescence spectrophotometer (Jobin Yvon, France), with a CW NIR laser at λ=980 nm as the excitation source. The Fourier transform infrared (FTIR) spectra were recorded on a Nicolet 5700 Fourier transform infrared spectrometer within the range of 500-4000cm^{-1}. Diffuse reflection spectrums of pure and modified films were

observed on Carry 5000. The incident photon conversion efficiency (IPCE) was measured using a 150 W xenon lamp (Oriel) fitted with a monochromator (Cornerstone 74004) as a monochromatic light source. IPCE photocurrents were recorded under short-circuit conditions using a Newport 2931-C power meter. Photocurrent voltage $I-V$ measurements were performed using a Newport $I-V$ tester (Oriel Class A 91160A) at 1 sun condition (100 mW/cm^2 at AM1.5). The irradiated area of each cell was kept at 0.25 cm^2 by using a light-tight metal mask. Dye loading measurements were conducted by immersing the films in 0.1 M NaOH solution and monitoring the concentration of desorbed dye by UV/vis spectroscopy. Quantum yield measurement was performed using a fluorescence spectroscopy (Edinburgh LFS920) modified by using Ocean Optics UV-VIS-NIR CCD (QE65000) as a detector for collecting the 980 nm light and the UC emissions. An integrating sphere was also used to measure the efficiency data. The response of the detection systems in photon flux was determined using a calibrated VIS-NIR lamp (Ocean Optics LS-1-CAL). For the lifetime characterization, direct excitation into the infrared (980 nm), green (Er^{3+} $^4S_{3/2}$ at 543 nm) emitting states was performed by phosphorescence lifetime spectrometer (FSP920-C, Edinburgh) equipped with a tunable mid-band OPO pulse laser as excitation source (410-2400 nm, 10 Hz, pulse width ≤ 5 ns, Vibrant 355II, OPOTEK).

3. Results and discussion

In order to investigate the structure of as-synthesized samples, XRD was employed to analyze the products. Figure 2 shows the XRD patterns for as-prepared $NaYF_4$:Yb,Er NPs, $NaYF_4$:Yb,Er @SiO_2 NPs, $NaYF_4$:Yb,Er@SiO_2@Au powder samples. The diffraction peaks in curve a can be indexed as a pure hexagonal $NaYF_4$:Yb,Er NPs (JCPDS card 28-1192).[39] After coating with the silica layer, the diffraction pattern of the resulting material (curve b) shows a reflection characteristic of amorphous SiO_2 in addition to the $NaYF_4$:Yb,Er diffraction peaks. The XRD pattern of the $NaYF_4$@SiO_2@Au nanocomposites (curve c) exhibits the superimposition of reflections of $NaYF_4$ phase and Au phase. The four peaks position at 2θ values of 38.2º, 44.4º, 64.7º, and 77.7º, which correspond to the (111), (200), (220), and (311) lattice planes of the cubic phase Au (JCPDS card 04-0784), respectively. This preliminarily proves the successful preparation of $NaYF_4$:Yb,Er@SiO_2@Au nanocomposites.

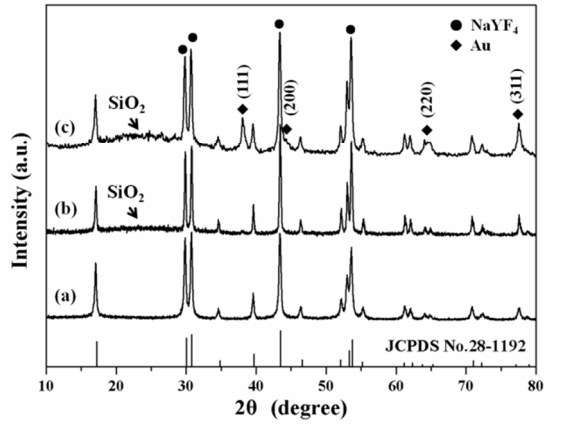

Figure 2. XRD patterns for prepared (a) $NaYF_4$:Yb,Er, (b) $NaYF_4$:Yb,Er@SiO_2 and (c) $NaYF_4$:Yb,Er@SiO_2@Au samples.

Figure 3a shows the SEM image of Yb, Er codoped $NaYF_4$ UCNPs. As can be seen from a low magnification SEM image, these UCNPs exhibit perfect uniformity and monodispersity, analysis of them reveal that they have an average size of ~270 nm in length and ~200 nm in width, the surfaces of them are very rough. To isolate upconversion core with the external environment, a uniform silica layer was coated on their surfaces by a typical modified Stöber sol-gel process.[42] As given in Figure 3b, the core single-shell structure can be observed clearly with the amorphous SiO_2 shell thickness around 15 nm, and the surfaces of them are smooth. After aminosilane was grafted onto the silica layer, the existence of amino groups provides a powerful claw for the $NaYF_4$:Yb,Er@SiO_2 NPs to grab Au NPs, due to the strong coordination between Au NPs and the -NH_2 group. It is observed from Figure 3c and d that Au NPs have good monodispersity and an average size about 20 nm. Figure 3e presents typical TEM image of the core-shell-structured $NaYF_4$:Yb,Er@SiO_2@Au nanocomposites. It can be seen that all Au NPs had been attached to the $NaYF_4$:Yb,Er@SiO_2 NPs and no free Au NPs had been found nearby. In the EDS spectrum (Figure 3f), besides the peaks of host (Na, Y, F) and dopants (Yb, Er), Si, O and Au elements were also detected in the $NaYF_4$:Yb,Er@SiO_2@Au nanocomposites.

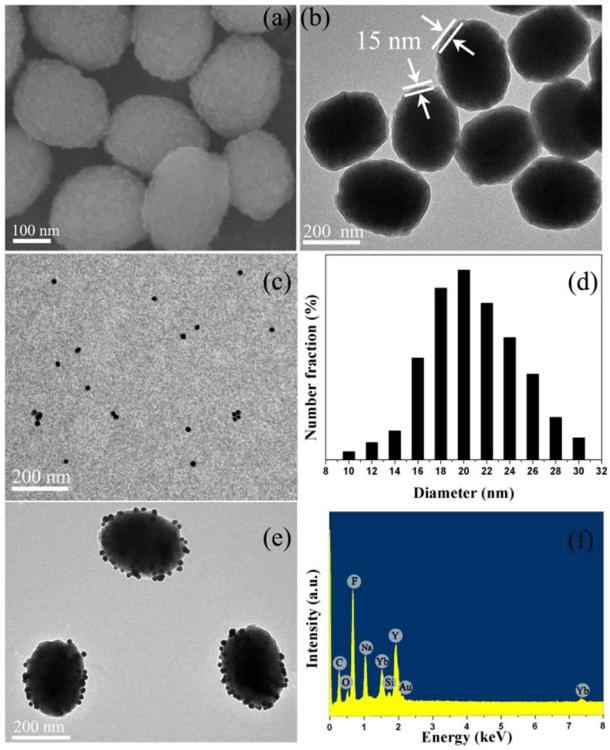

Figure 3. (a) SEM image of $NaYF_4$:Yb,Er NPs. TEM images of (b) $NaYF_4$@SiO_2 NPs, (c) Au NPs, (e) $NaYF_4$@SiO_2@Au nanocomposites. (d) Histogram of the corresponding diameter distribution of Au NPs. (f) EDS spectrum of obtained $NaYF_4$@SiO_2@Au nanocomposites.

The UV-vis absorption spectra of Au NPs, $NaYF_4$:Yb,Er NPs and $NaYF_4$:Yb,Er@SiO_2@Au nanocomposites are shown in Figure 4a. It is known that for Au NPs in sizes ranging from 2 to 100 nm, the electrons are trapped in the small Au metal box and exhibit a characteristic of collective oscillation frequency of the plasmon resonance, giving rise to the LSPR band at around 520

nm.[43] The broad absorption band peaked at 530 nm in the spectrum of $NaYF_4$:Yb,Er@SiO_2@Au indicates the presence of Au NPs, a slight red shift is observed compared to bare Au NPs, this observation is also consistent with previous report that the LSPR peak would shift to higher wavelengths with the aggregation of Au NPs.[44]

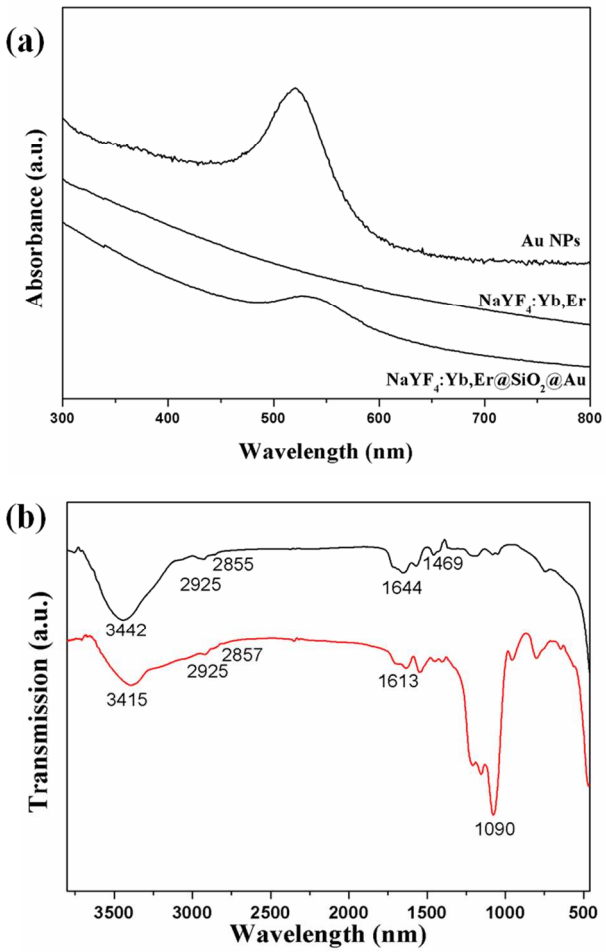

Figure 4. (a) UV-vis absorption spectra of Au NPs, $NaYF_4$:Yb,Er NPs and $NaYF_4$:Yb,Er@SiO_2@Au nanocomposites. (b) FTIR spectra of PAA modified-$NaYF_4$:Yb,Er NPs (black curve), APTMS modified-$NaYF_4$:Yb,Er@SiO_2 NPs (red curve).

The surfaces of UCNPs without modification are coated with a layer of PAA, which can be confirmed by the FTIR spectroscopy in Figure 4b. It is observed in curve a, the PAA exhibits a transmission band at around 3442 cm^{-1}, corresponding to the stretching vibration of hydroxyl group. Two peaks at 1644 and 1469 cm^{-1} are associated with the asymmetric and symmetric stretching vibrations of the carboxylic group (COO^-), respectively.[45] In addition, the two peaks at 2925 and 2855 cm^{-1} can be assigned to the asymmetric and symmetric stretching vibrations of methylene group, respectively, which exists in the long alkyl chain of the PAA molecule. Curve b shows the FTIR spectrum of the amino-modified $NaYF_4$:Yb,Er@SiO_2 NPs. The stretching and bending vibration bands of amine group appear at 3415 and 1613 cm^{-1} in the spectrum, respectively. A strong transmission band attributed to the symmetrical stretching vibration of the Si-O bond can be seen clearly at 1090 cm^{-1} in the spectrum.[46] In addition, the two peaks at 2925 and 2857 cm^{-1} are corresponding to the asymmetric and symmetric stretching vibrations of methylene group, respectively, which exists in the hydrolysate of APTMS. The peak at 1097 cm^{-1} suggests that the UCNPs were successfully coated with a layer of silica, whereas the peaks at 3415, 2925, and 2857 cm^{-1} together verify the silica-coated UCNPs have been functionalized with amino groups.

Upconversion fluorescence spectra of the as-prepared samples are shown in Figure 5. The inset image shows the upconversion fluorescence photograph of obtained $NaYF_4$:Yb,Er@SiO_2@Au nanocomposites in water under excitation of a 980 nm laser. Two green peaks (525 and 543 nm) and a red peak (655 nm) are ascribed to the energy transitions from $^2H_{11/2}$, $^4S_{3/2}$ and $^4F_{9/2}$ to $^4I_{15/2}$ of Er^{3+} ions, respectively, when excited under a commercial continuous wave diode NIR laser. After the UCNPs were coated with the silica layer and modified with amino groups, their fluorescence decreased to some extent because of the light scattering effects on both emission and incident light by the silica layer. However, with Au NPs attachment, remarkable enhancement for multicolour upconversion emission was observed, and an enhancement factor of more than 2 was achieved. The quantum yield obtained by integrated sphere is 0.023 ± 0.01% for $NaYF_4$:Yb,Er NPs and the decay curves of Er^{3+} emission at 543 nm in $NaYF_4$:Yb,Er and $NaYF_4$:Yb,Er@SiO_2@Au samples were measured using 980 nm excitation. As shown in Figure S1 (ESI†), the lifetimes of the $^4S_{3/2}\rightarrow{}^4I_{15/2}$ transition of Er^{3+} were measured to be 32.4 μs and 57.9 μs for $NaYF_4$:Yb,Er and $NaYF_4$:Yb,Er@SiO_2@Au, respectively, suggesting that the emission yield is enhanced following attachment of Au NPs. This result is consistent with the upconversion fluorescence spectra shown in Figure 5. The enhancement effects from Au NPs can be attributed to at least two possible factors. (1) Increase of the excitation rate by local field enhancement, which is an enhancement of the effective excitation flux caused by local field enhancement.[47] (2) Increase of the emission rate by surface plasmon-coupled emission (SPCE), which will increase both the nonradiative and radiative decay rate of fluorophores. SPCE could occur when the plasmon resonance frequency overlaps with the emission band of fluorophores. UV-vis absorption spectrum of the Au NPs (Figure S2, ESI†) clearly show that the plasmonic resonance frequency of the Au NPs overlaps well with the green and red emission of the upconversion emission. This allows the effective coupling of LSPR of Au NPs with upconversion emission, therefore, the radiative decay rate and emission intensity of the UCNPs will be increased.[36]

In order to investigate the DSSCs performance of these samples, a bilayer film was constructed by printing a layer (~5 μm) of samples on the top of a layer of (~7.5 μm) of TiO_2.[48] For clarity, samples are denoted as T, T/N, T/N@S, T/N@S@A, where T and N represent pure TiO_2 and $NaYF_4$:Yb,Er crystal, S and A mean the inner SiO_2 and outer Au shell, respectively. The photocurrent density-voltage curves (*J-V*) of DSSCs based on different photoelectrode are shown in Figure 6a, and their photovoltaic parameters are summarized in Table 1. It can be seen that the pure T cell exhibites a short-circuit current density (J_{sc}) of 13.63 mA cm^{-2} and an efficiency (η) of 7.17%. Nevertheless, due to the serious recombination effects from bare

Cite this: DOI: 10.1039/c0xx00000x

www.rsc.org/xxxxxx

ARTICLE TYPE

Table 1. Detailed photocoltaic characteristics and dye loading properties of DSSCs based on different photoanodes

Device	J_{sc} (mA cm^{-2})	V_{oc} (V)	Fill Factor (%)	η (%)	Dye loading (×10^{-7} mol cm^{-2})
T	13.63	0.77	67.80	7.17	1.08
T/N	11.90	0.78	63.16	5.80	1.04
T/N@S	14.78	0.79	65.83	7.56	1.11
T/N@S@A	15.84	0.80	65.72	8.23	1.07

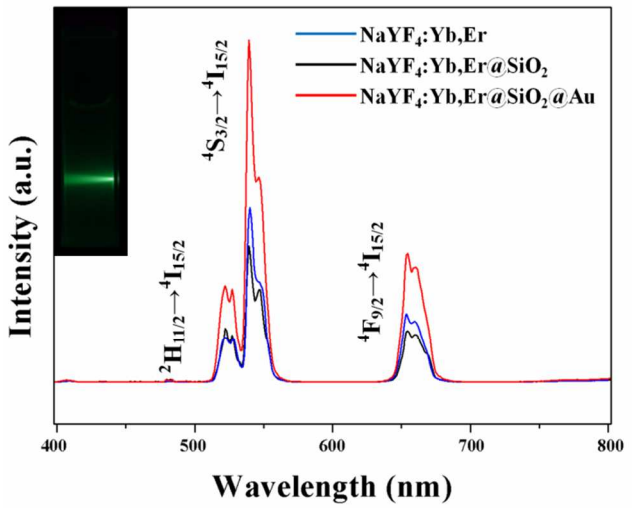

Figure 5. Upconversion fluorescence spectra of the $NaYF_4$:Yb,Er, $NaYF_4$:Yb,Er@SiO_2 and $NaYF_4$:Yb,Er@SiO_2@Au nanoparticles. The inset is digital photograph of upconversion fluorescence of $NaYF_4$:Yb,Er@SiO_2@Au under excitation of a 980 nm laser. All the samples at 0.5 mg mL^{-1} were used in the experiment.

UCNPs, device T/N shows the lowest J_{sc} of 11.90 mA cm^{-2}, and η of 6.77%, despite the light harvesting capability. Then, after of 6.77%, despite the light harvesting capability. Then, after being coated with the thin SiO_2 insulating layer (T/N@S), the negative recombination effects would be avoided and J_{sc} is greatly enhanced to 14.78 mA cm^{-2} benefitting from the minor upconversion effects and the predominant light scattering effects,[49] since the upconversion contribution has been proved almost negligible due to low quantum yield of upconversion materials.[26] With coating of Au NPs, the performance was optimized and the highest J_{sc} of 15.84 mA cm^{-2} and η of 8.23% were achieved, which are 14.78% enchancement in efficiency compared to bare TiO_2 crystals and 8.86% increasement compared to the device based on $NaYF_4$:Yb,Er@SiO_2 crystals. The enhancement is believed to be associated with enhanced scattering effects by incorporating with these effective scattering centers and more photoinduced electrons from these upconversion centers, and LSPR effects from incorporated Au NPs.

Detailed information on the light harvesting of the DSSCs can be obtained from the incident-photon-to-current conversion efficiency (IPCE) spectra (Figure 6b).[50] For device T/N, as large number of photoinduced electrons were traped by surface defects and ligands on these bare T crystals, less electrons were recaptured by I_3^-, device T/N exhibts the lowest IPCE performance. By adding of the insulating SiO_2 layer and attaching Au NPs, it can be seen that the IPCE values were considerably reinforced in the entire visible region, and the device T/N@S@A possesses the highest IPCE values. Compared to devive T/N@S, the higher IPCE values of device T/N@S@A are considered as in plasmon enhanced solar cells, plasmon excitation could improve optical density near the metal surfaces, dye molecules located in the vicinity of the nanoparticles can harvest more photons, thus increasing the IPCE.[51,52] Hence, these results confirm the significant optoelectronic benefits from the $NaYF_4$:Yb,Er@SiO_2@Au nanocomposites layer in the cell design and is reflected in the remarkable efficiency enhancement.

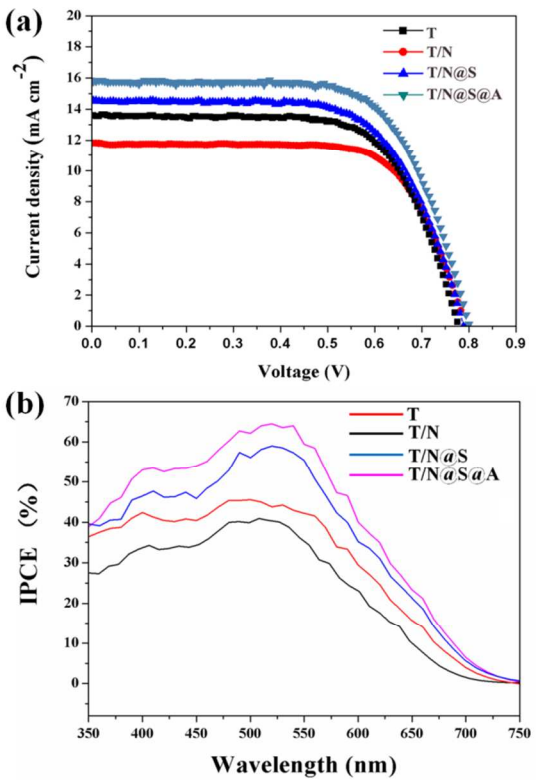

Figure 6. *J–V* curves (a) and IPCE spectra (b) of DSSCs with different photoanodes.

Light scattering properties of unsensitized photoanodes were evaluated by measuring the diffuse reflectance. As given in Figure 7a, by comparison with the transparent TiO_2 film, bilayer films are found have remarkable improvement in light reflectance

over the entire region, indicating the large dimension nanocomposites can act as effective light scattering centers to extend of light path-length within the electrodes,[26] thus increase of light harvesting. Thereby, the outstanding efficiency value of device T/N@S@A is partially given rise by an enhanced light harvesting due to outstanding light scattering and reflecting effects. Hence, superior light scattering ability (Figure 7a), enhanced upconversion emission (Figure 5, red line) and high IPCE values (Figure 6b), which together produce an enhanced J_{sc} (15.84 mA cm^{-2}) and an improved η (8.23%) for the device T/N@S@A, as compared to other devices in this work.

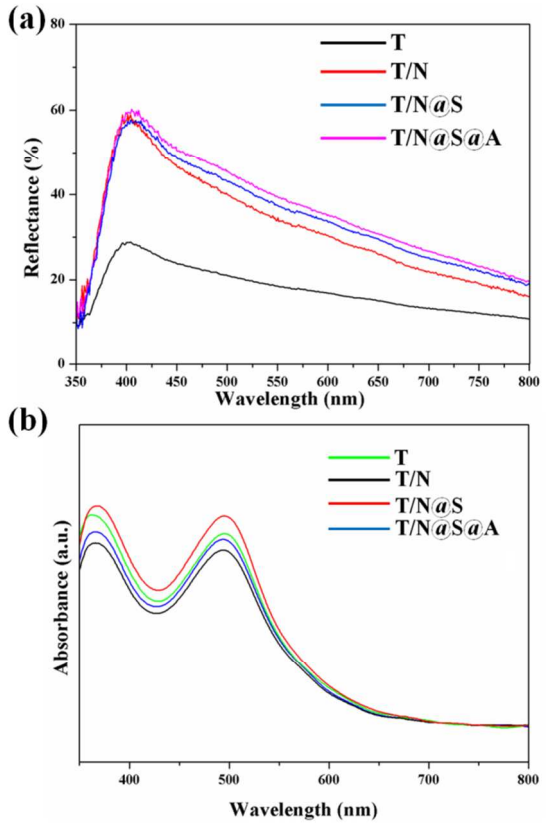

Figure 7. (a) UV-vis diffuse reflectance spectra with different photoanodes and (b) UV-vis absorption spectra of N719 dye in 0.1 M NaOH aqueous solution, desorbed from different photoanodes.

To further identify the effects of LSPR, the absorbed dye concentration on the samples surface was quantified by desorbing the N719 dye from the sample electrodes in an alkaline aqueous medium. Absorption spectra of the N719 dye in 0.1 M NaOH aqueous solution are shown in Figure 7b. It can be seen that the device T/N@S has the highest dye loading amount (due to abundant surface silanols), however, the increased dye loading amount will not contribute to photocurrent by charge injection *via* dye on the SiO_2 surface, but the increase of J_{sc} mainly come from increased scattering. The amount of dye adsorption decreased after Au NPs modification compared to device T/N@S, indicating the improvement of J_{sc} in case of device T/N@S@A could be attributed to combined effects of LSPR and enhanced upconversion effects rather than excess dye loading. For LSPR effects, oscillating conduction electrons of Au NPs resonate with the electric field of incident light, resulting in enhancement of the oscillating electric fields that are localized in the vicinity of Au NPs. The localized electric fields can excite dyes more effectively than the incident far-field light. [53]

The possible mechanism of enhanced light trapping can be described with reference to the schematic of Figure 8. When the light reaches the $NaYF_4$:Yb,Er@SiO_2 NPs layer in an actual solar cell, it is randomized in terms of directions by scattering in the TiO_2 layer. It will get back-scattered (dashed red arrows) due to better scattering ability of large dimension of the samples. Upconversion fluorescence emission will happen simultaneously

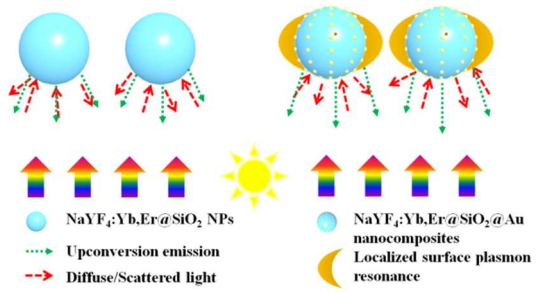

Figure 8. The mechanism of light harvesting in the case of $NaYF_4$:Yb,Er@SiO_2 NPs and $NaYF_4$:Yb,Er@SiO_2@Au nanocomposites respectively.

thanks to strong NIR light from solar radiation (dashed green arrows). In the case of $NaYF_4$:Yb,Er@SiO_2@Au nanocomposites layer, when light interacts with the embedded Au NPs, it can generate LSPR which can concentrate electromagnetic fields leading to trapping of the light effectively. Furthermore, the coupled LSPR can travel about micron distances from their origin point, hence the energy transfer to the dye molecules could also be enhanced.[34] Additionally, the LSPR helps in concentrating the light in the device interior as well. Meanwhile, the intensity of upconversion emission could be enhanced, upconversion effects could be enhanced at the same time.

4. Conclusions

In conclusion, core-shell-structured β-$NaYF_4$:Yb,Er@SiO_2@Au hybrid nanocomposites were successfully prepared and employed for proof-of-concept study in DSSCs internally as a multifunctional layer on top of the transparent TiO_2 layer. Due to their large dimension, these nanocomposites can act as effective scattering centers to enhance the light harvesting. By coating with amorphous SiO_2 insulating layer around the β-$NaYF_4$:Yb,Er NPs, the electron trapping and capture caused by surface defects and ligands of bare β-$NaYF_4$:Yb,Er crystals can be thoroughly avoided. After attachment of Au NPs, the performance of DSSCs was significantly enhanced, resulting in efficiency of 8.23%, which is a noticeable improvement of 14.78% compared to the device without the multifunctional layer (7.17%). This is most likely caused by the combined effects of light scattering, LSPR and enhanced upconversion. Therefore, we outline a facile strategy for incorporating LSPR with upconversion effects to further optimize the efficiency of DSSCs.

Acknowledgements

This work was supported by the National Natural Science

Foundation of China (21236003, 21206042, 20925621, and 21176083), the Basic Research Program of Shanghai (13NM1400700, 13NM1400701), and the Fundamental Research Funds for the Central Universities.

References

Key Laboratory for Ultrafine Materials of Ministry of Education, School of Materials Science and Engineering, East China University of Science and Technology, Shanghai 200237, China. Fax: +86 21 6425 0624; Tel: +86 21 6425 2022; E-mail: yhzhu@ecust.edu.cn *and czli@ecust.edu.cn*

† Electronic Supplementary Information (ESI) available: additional Figures as noted in the text. See DOI: 10.1039/b000000x/

1 B. O'Regan, M. Grätzel, *Nature,* 1991, **353**, 737.
2 Y. Hou, D. Wang, X. H. Yang, W. Q. Fang, B. Zhang, H. F. Wang, G. Z. Lu, P. Hu, H. J. Zhao, H. G. Yang, *Nat. Commun.*, 2013, **4**, 1583.
3 B. Liu and E. S. Aydil, *J. Am. Chem. Soc.*, 2009, **131**, 3985.
4 M. Ye, C. Chen, M. Lv, D. Zheng, W. Guo and C. Lin, *Nanoscale*, 2013, **5**, 6577.
5 J. T. Park, W. S. Chi, H. Jeon and J. H. Kim, *Nanoscale*, 2014, **6**, 2718.
6 S. R. Gajjela, C. Yap and P. Balaya, *J. Mater. Chem.*, 2012, **22**, 10873.
7 H. C. Pang, H. B. Yang, C. X. Guo, J. L. Lu and C. M. Li, *Chem. Commun.*, 2012, **48**, 8832
8 K. E. Lee, C. Charbonneau and G. P. Demopoulos, *J. Mater. Res.*, 2013, **28**, 480.
9 G. Zhu, X. J. Wang, H. L. Li, L. K. Pan, H. C. Sun, X. J. Liu, T. Lv and Z. Sun, *Chem. Commun.*, 2012, **48**, 958.
10 G. B. Shan, G. P. Demopoulos, *Adv. Mater.,* 2010, **22**, 4373.
11 T. Trupke, M. A. Green, P. Würfel, *J. Appl. Phys.,* 2002, **92**, 4117.
12 V. Badescu, A. M. Badescu, *Renewable Energy,* 2009, **34**, 1538.
13 J. Wu, J. Wang, J. Lin, Z. Lan, Q. Tang, M. Huang, Y. Huang, L. Fan, Q. Li, Z. Tang, *Adv. Energy Mater.,* 2012, **2**, 78.
14 B. Wu, X. Wu, C. Guan, K. F. Tai, E. K. L. Yeow, H. J. Fan, N. Mathews, T. C. Sum, *Nat. Commun.*, 2013, **4**, 2004.
15 G. X. Xie, J. M. Lin, J. H. Wu, Z. Lan, Q. H. Li, Y. M. Xiao, G. T. Yue, H. F. Yue, M. L. Huang, *Chin. Sci. Bull.,* 2011, **56**, 96.
16 S. Gai, P. Yang, C. Li, W. Wang, Y. Dai, N. Niu, and J. Lin, *Adv. Funct. Mater.*, 2010, **20**, 1166.
17 G. Shan, H. Assaaoudi, G. P. Demopoulos, *ACS Appl. Mater. Interfaces,* 2011, **3**, 3239.
18 A. Aebischer, M. Hostettler, J. Hauser, K. Kramer, T. Weber, H.U. Gudel, H.B. Burgi, *Angew. Chem. Int. Ed.,* 2006, **45**, 2802.
19 J. F. Suyver, A. Aebischer, S. Garcia-Revilla, P. Gerner, H. U. Gudel, *Phys. Rev. B*, 2005, **71**, 125123.
20 G. Y. Chen, T. Y. Ohulchanskyy, R. Kumar, H. Agren, P. N. Prasad, *ACS Nano*, 2010, **4**, 3163.
21 D. J. Gargas, E. M. Chan, A. D. Ostrowski, S. Aloni, M. V. P. Altoe, E. S. Barnard, B. Sanii, J. J. Urban, D. J. Milliron, B. E. Cohen and P. J. Schuck, *Nat. Nanotechnol.*, 2014, **9**, 300.
22 X. Ye, J. E. Collins, Y. Kang, J. Chen, D. T. N. Chen, A. G. Yodh, and C. B. Murray, *PNAS*, 2010, **107**, 22430.
23 M. Haase, H. Schäfer, *Angew. Chem. Int. Ed.,* 2011, **50**, 5808.
24 H. X. Mai, Y. W. Zhang, L. D. Sun, C. H. Yan, *J. Phys. Chem. C,* 2007, **111**, 13721.
25 F. Wang, J. Wang, X. Liu, *Angew. Chem.Int. Ed.,* 2010, **122**, 7618.
26 L. Liang, Y. Liu, C. Bu, K. Guo, W. Sun, N. Huang, T. Peng, B. Sebo, M. Pan, W. Liu, S. Guo, and X. Zhao, *Adv. Mater.,* 2013, **25**, 2174.
27 M. D. Brown, T. Suteewong, R. S. S. Kumar, V. D'Innocenzo, A. Petrozza, M. M. Lee, U. Wiesner, H. J. Snaith, *Nano Lett.*, 2011, **11**, 438.
28 W. Jiang, H. Liu, L. Yin and Y. Ding, *J. Mater. Chem. A*, 2013, **1**, 6433.
29 B. Ding, B. J. Lee, M. J. Yang, H. S. Jung and J. K. Lee, *Adv. Energy Mater.*, 2011, **1**, 415.
30 D. Paz-So1dan, A. Lee, S. M. Thon, M. M. Adachi, H. Dong, P. Maraghechi, M. Yuan, A. J. Labelle, S. Hoogland, K. Liu, E. Kumacheva, and E. H. Sargen, *Nano Lett.*, 2013, **13**, 1502.
31 X. Ye, C. Zheng, J. Chen, Y. Gao, and C. B. Murray, *Nano Lett.*, 2013, **13**, 765.
32 H. Li, K. Yuan, Y. Zhang, and J. Wang, *ACS Appl. Mater. Interfaces*, 2013, **5**, 5601.
33 V. E. Ferry, L. A. Sweatlock, D. Pacici and H. A. Atwater, *Nano Lett.*, 2008, **8**, 4391.
34 R. A. Naphade, M. Tathavadekar, J. P. Jog, S. Agarkar, S. Ogale, *J. Mater. Chem. A*, 2014, **2**, 975.
35 N. Liu, W. Qin, G. Qin, T. Jiang and D. Zhao, *Chem. Commun.*, 2011, **47**, 7671.
36 P. Zhao, Y. Zhu, X. Yang, K, Fai, J. Shen and C. Li, *RSC Adv.*, 2012, **2**, 10592.
37 Y. Liu, H. Zhai, F. Guo, N. Huang, W. Sun, C. Bu, T. Peng, J. Yuan and X. Zhao, *Nanoscale*, 2012, **4**, 6863.
38 P. Zhao, Y. Zhu, X. Yang, J. Shen, X. Jiang, J. Zong and C. Li, *Dalton Trans.*, 2014, **43**, 451.
39 P. Zhao,Y. Wu, Y. Zhu, X. Yang, X. Jiang, J. Xiao, Y. Zhang and C. Li, *Nanoscale*, 2014, **6**, 3804.
40J. Kimling, M. Maier, B. Okenve, V. Kotaidis, H. Ballot and P. Plech, *J. Phys. Chem. B*, 2006, **110**, 15700.
41 R. L. Willis, C. Olson, B. O'Regan, T. Lutz, J. Nelson, J. R. Durrant, *J. Phys. Chem. B,* 2002, **106**, 7605.
42 W. Stöber, A. Fink, E. Bohn, *J. Colloid Interface Sci.,* 1968, **26**, 62.
43 C. Daniel, D. Astruc, *Chem. Rev.*, 2004, **104**, 293.
44 J. W. Bai, S. X. Huang, L. Y. Wang, Y. Chen, Y. Huang, *J. Mater. Chem.*, 2009, **19**, 921.
45 M. Wang, C. C. Mi, W. X. Wang, C. H. Liu, Y. F. Wu, Z. R. Xu, C. B. Mao, and S. K. Xu, *ACS Nano*, 2009, **3**, 1580.
46 M. Wang, W. Hou, C. C. Mi, W. X. Wang, Z. R. Xu, H. H. Teng, C. B. Mao, and S. K. Xu, *Anal. Chem.*, 2009, **81**, 8783.
47 H. Zhang, Y. Li, I. A. Ivanov, Y. Qu, Y. Huang, and X. Duan, *Angew. Chem. Int. Ed.*, 2010, **49**, 2865.
48 J. Huo, Y. Hu, H. Jiang, W. Huang, Y. Li, W. Shao, and C. Li, *Ind. Eng. Chem. Res.*, 2013, **52**, 11029.
49 L. Liang, Y. Liu and X. Zhao, *Chem. Commun.*, 2013, **49**, 3958.
50 F. Z. Huang, D. H. Chen, X. L. Zhang, R. A. Caruso and Y. B. Cheng, *Adv. Funct. Mater.*, 2010, **20**, 1301.
51 I. K. Ding, J. Zhu, W. S. Cai, S. J. Moon, N. Cai, P. Wang, S. M. Zakeeruddin, M. Gräetzel, M. L. Brongersma, Y. Cui and M. D. McGehee, *Adv. Energy Mater.*, 2011, **1**, 52.
52 J. Qi, X. Dang, P. T. Hammond and A. M. Belcher, *ACS Nano*, 2011, **5**, 7108.
53 W. B. Hou, P. Pavaskar, Z. W. Liu, J. Theiss, M. Aykol and S. B. Cronin, *Energy Environ. Sci.*, 2011, **4**, 4650.